

Article

# Polynomial Cancellation Coded DFT-s-OFDM for Low-PAPR Uplink Signaling

Li Cho <sup>1,\*</sup> , Yu-Ming Kuo <sup>1</sup>, Yi-Shin Wu <sup>2</sup> and Chau-Yun Hsu <sup>1,2</sup>

<sup>1</sup> Graduate Institute of Communication Engineering, Tatung University, Taipei 10452, Taiwan; g10610010@ms.ttu.edu.tw (Y.-M.K.); cyhsu@gm.ttu.edu.tw (C.-Y.H.)

<sup>2</sup> Department of Electrical Engineering, Tatung University, Taipei 10452, Taiwan; d10702001@ms.ttu.edu.tw

\* Correspondence: d10510001@ms.ttu.edu.tw; Tel.: +886-2-2182-2928

Received: 4 October 2019; Accepted: 13 November 2019; Published: 14 November 2019



**Abstract:** The physical layer signaling of the 5G new radio still utilizes cyclic prefix orthogonal frequency division multiplexing (CP-OFDM) and discrete Fourier transform-spread-OFDM (DFT-s-OFDM) to support 5G services for the sake of system-backward compatibility. However, the transmission requirements among these services differ, and this poses a challenge to the adaptability of the waveforms with regard to the peak-to-average power ratio (PAPR) issue. In particular, DFT-s-OFDM serving as a low-PAPR option for uplink signaling still has room for PAPR improvement in cases such as machine-type and device-to-device communications. We propose polynomial cancellation coded (PCC)-DFT-s-OFDM to flexibly reduce the PAPR of conventional DFT-s-OFDM. The principle of the proposed method, including its transform, is analyzed in the time domain. The results show that it can also be regarded as a novel spectral shaping scheme for PAPR reduction. Through a parameter designed for adjusting the cost of spectral efficiency, the proposed method can regulate the extent of improvement compared with the conventional DFT-s-OFDM, not only in the PAPR, but also for the spectral radiation and bit error rate when considering the nonlinearity of the power amplifier. The increase in computational complexity is neglectable owing to the simplicity of generalized PCC, making it apt to be deployed in existing systems.

**Keywords:** discrete fourier transform spread orthogonal frequency division multiplexing (DFT-s-OFDM); peak-to-average power ratio (PAPR); polynomial cancellation coding (PCC); 5G waveform; spectrum shaping; moving filter

## 1. Introduction

Orthogonal frequency division multiplexing (OFDM) underlies modern wireless communication systems such as IEEE 802.11 a/g/n/ac wireless local area networks (WLANs), digital audio broadcasting (DAB), digital video broadcasting (DVB), fourth-generation (4G) cellular networks (e.g., long-term evolution/LTE and worldwide interoperability for microwave access/WiMAX), and the 5G new radio (NR) [1–3]. However, the high peak-to-average power ratio (PAPR) problem [4] of OFDM remains a long-standing implementation issue [5–8]. Many studies have considered how to operate the transmit power amplifier (PA) in its linear region with less input backoff (IBO). That is, to be more power-efficient.

Although reducing the PAPR of the signal is an issue both at the uplink and downlink, it is more critical for the uplink, owing to the limited cost and power-budget of user equipment. As PAs are one of the most energy-hungry components of a user equipment transceiver, the energy efficiency can be improved by efficient PA conversion, which can extend the battery life of the user equipment. Alternatively, it can significantly boost the transmission power to increase the number of cell-edge users and the signal-to-noise ratio (SNR) at the same IBO [9]. Therefore, PAPR has been regarded as one of the requirements of waveform design for 5G and beyond [10–12]. Nevertheless, the Third Generation

Partnership Project (3GPP) still uses the cyclic prefix (CP)-OFDM and discrete Fourier transform-spread OFDM (DFT-s-OFDM) as the waveforms of 5G NR [3]. This postpones many waveform candidates such as filter-bank multicarrier (FBMC), generalized frequency division multiplexing (GFDM), universal filtered multicarrier (UFMC), windowed-OFDM (W-OFDM), and filtered-OFDM (F-OFDM) [12,13], mainly owing to their high-PAPR essence and low LTE compatibility.

The importance of backward compatibility can be also reflected in PAPR reduction schemes for 3GPP standards. Various PAPR reduction methods are described in the literature [5–8]. However, only two have been agreed upon as standard solutions for 4G LTE and 5G NR uplink signaling [2,3]. The first standard solution, DFT-s-OFDM, which is also known as single-carrier frequency-division multiple access (SC-FDMA), appeared in 2006 [14]. It was used to conduct relatively low-PAPR signaling by only reusing the chip-built-in DFT module in user equipment. The second solution is rotated modulation, including  $\pi/2$ -binary phase shift keying ( $\pi/2$ -BPSK) and  $\pi/4$ -quadrature PSK ( $\pi/4$ -QPSK), which were originally adopted for narrow-band internet of things (NB-IoT) mono-tone transmissions since Rel-13 [15]. Apart from the QPSK and quadrature amplitude modulations (QAMs),  $\pi/2$ -BPSK has been a part of the available modulations of the DFT-s-OFDM uplink since Rel-15 [3]. The  $\pi/2$ -BPSK and  $\pi/4$ -QPSK perform identically in terms of errors to BPSK and QPSK, but reduce the PAPR without any increase in computational complexity, making it highly compatible with the current waveforms.

However, the PAPR performance of the current standard solution is fixed and cannot be further improved if the communication scenario values the PAPR than other performances. Therefore, it is important to establish a mechanism to adjust a signal's PAPR in a flexible manner that ensures a sufficient trade-off between spectral efficiency and energy efficiency (in PAPR aspect) in 5G [16]. The device capabilities for each 5G use case, including enhanced mobile broadband (eMBB), ultra-reliable and low latency communications (URLLC), and massive machine type communications (mMTC) are quite different [17]. For example, reducing the PAPR of a signal can directly increase the reliability for URLLC owing to the increased SNR, but can lower the signal nonlinearity and power consumption for mMTC devices, which are usually only equipped with basic PA. Nonlinear uplink signals bring severe interferences between users, particularly those with narrowband transmissions. Furthermore, since the sidelink used for proximity services (ProSe) in device-to-device (D2D) communication has been defined as a subset of the uplink resources [18], the issue of D2D power control critically challenges system performance [16,19]. This is because the D2D network dynamically connects various types of user equipment (i.e., various qualities of PA) to support different scenarios of ProSe. DFT-s-OFDM signaling is expected to be a more robust waveform for uplink through adjustable PAPR reduction schemes. Hence, several data-independent schemes such as spectral shaping (SS) [20], which use extra subcarriers to further reduce PAPR, have been investigated to overcome the need for a flexible countermeasure to the PAPR problem [16,21]. Although the results in [16] successfully achieved 2–3 dB PAPR reduction compared with conventional DFT-s-OFDM with 10%–20% spectral efficiency loss, further spectral efficiency loss does not improve the PAPR performance more, and instead degrades it.

In addition, a long-established OFDM-based waveform, polynomial cancellation coding (PCC)-OFDM [22], is developed for reducing the out-of-band (OOB) interference between users. The PCC applied in PCC-OFDM is treated as a frequency coding technique for OFDM that maps the data onto weighted groups of subcarriers. With this simple preprocessing, the differential operation in the time domain benefits PCC-OFDM on the performance of frequency localization, and the immunity of frequency offset and Doppler spread, making it one of the waveform candidates for 5G and beyond [23]. As taking PCC in the data domain can shape the components in the transformed domain, this inspires us to exploit PCC as a novel SS scheme to reduce the PAPR of DFT-s-OFDM signals.

The goal of this paper is to further the idea of applying PCC on DFT-s-OFDM, i.e., PCC-DFT-s-OFDM, for improving the PAPR performance in a more flexible manner by making the following contributions:

- Time-domain transform and the SS function of PCC-DFT-s-OFDM are proposed for the PAPR reduction. By using the designed parameter to perform different orders of PCC, a wide range of trade-offs between spectral efficiency and energy efficiency performance can be achieved.
- The computational complexity of PCC-mapped DFT precoding matrix is analyzed. Comparing most of significant PAPR reduction techniques, e.g., selected mapping (SLM) [24] and partial transmit sequence (PTS) [25], the PCC increases complexity negligibly (add a simple subtractor circuit only) based on DFT-s-OFDM, which has been widely used in the uplink for existing LTE/NR systems.
- A comprehensive numerical simulation of the PCC-DFT-s-OFDM transceiver for a single user and multiple users in terms of PAPR, power spectral density (PSD) and bit error rate (BER) performances are provided. It shows that the PAPR of DFT-s-OFDM signals can be significantly reduced using the proposed method, thereby enhancing the PSD and BER, particularly when PA nonlinearity and inter-user interference are considered.

The rest of this paper is organized as follows. In Section 2, the system and signal model of the DFT-s-OFDM is described. In Section 3, we present the proposed PCC-DFT-s-OFDM with its principle of PAPR reduction from the viewpoints of both the time and frequency domains. An in-depth discussion of the properties of the proposed method and the results of simulations are provided in Section 4, which is followed by the concluding remarks.

## 2. System Model

Figure 1 shows a block diagram of a discrete baseband PCC-DFT-s-OFDM transceiver. In this study, we focus on localized FDMA [14] owing to the LTE/NR compatibility. Let  $\{s_r\}_{r=0}^{P-1}$ ,  $P \triangleq M/2^d$  be the input PSK/QAM symbols, where  $M$  is the number of allocated subcarriers and  $d \in \{0, 1, 2, \dots\}$  is the order of PCC. The PCC-mapped symbols can be expressed as:

$$v_m = s_{m/2^d} \cdot (-1)^{m \bmod 2^d}, 0 \leq m \leq M - 1, \tag{1}$$

where mod is the modulo operator. It is noteworthy that the PCC variable used is a general form, such that  $d = 0$  to disable the PCC mapping,  $d = 1$  for conventional PCC [22], and  $d \geq 2$  for higher-order PCC. Then, the PCC-mapped symbols are linearly precoded by an  $M$ -point DFT to result in the frequency-domain data  $X_k$ :

$$X_k = \frac{1}{\sqrt{M}} \sum_{m=0}^{M-1} v_m W_M^{km}, 0 \leq k \leq M - 1, \tag{2}$$

where  $W_M = e^{-j(\frac{2\pi}{M})}$  is the twiddle factor. After being zero-padded and after the  $N$ -point inverse DFT (IDFT) of  $X_k$  is taken, the transmitted signal samples  $x_n$  can be written as [26]:

$$\begin{aligned} x_n &= \frac{1}{\sqrt{N}} \sum_{k=0}^{M-1} X_k W_N^{-kn} \\ &= \frac{1}{\sqrt{MN}} \sum_{k=0}^{M-1} \sum_{m=0}^{M-1} v_m W_M^{km} W_N^{-kn} \\ &= \frac{1}{\sqrt{M}} \sum_{m=0}^{M-1} v_m g\left[n - \frac{N}{M}m\right], 0 \leq n \leq N - 1, \end{aligned} \tag{3}$$

where

$$g[n] = \frac{\sin\left(\frac{M\pi n}{N}\right)}{\sqrt{N}\sin\left(\frac{\pi n}{N}\right)} e^{j\frac{(M-1)\pi n}{N}}. \tag{4}$$

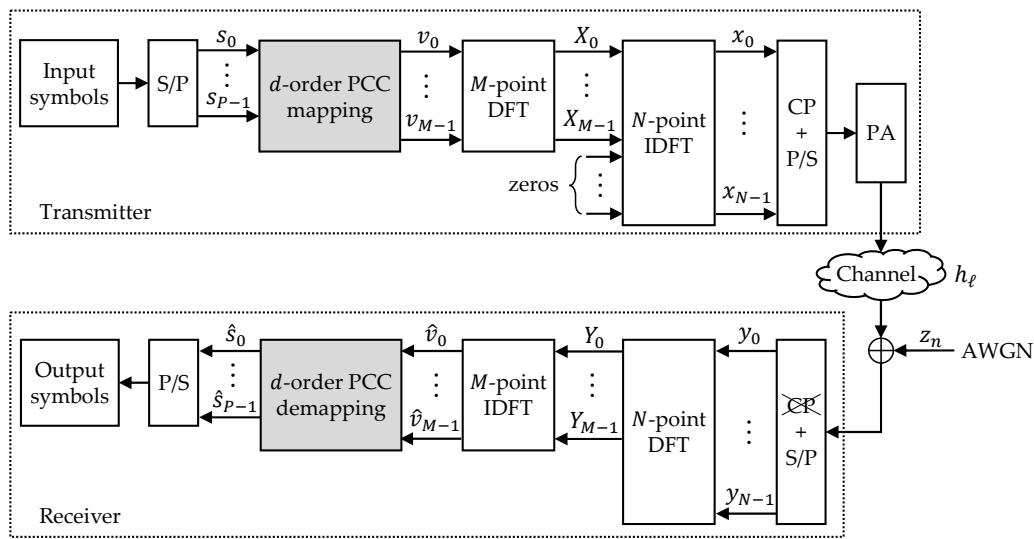


**Figure 1.** Block diagram of the discrete Fourier transform-spread orthogonal frequency division multiplexing (DFT-s-OFDM) transceiver with polynomial cancellation coding (PCC) mapping.

The performance of the PAPR  $\xi$  of the transmitted signal in terms of complementary cumulative density function (CCDF) can be presented as:

$$CCDF(\xi_0) = Pr(\xi > \xi_0), \quad \xi \triangleq \frac{\max_{0 \leq n \leq N-1} |x_n|^2}{\mathbb{E}\{|x_n|^2\}}, \quad (5)$$

where  $\mathbb{E}\{\bullet\}$  is the expectation operator.

Assuming the length of cyclic prefix (CP) is longer than the multipath channel impulse response, the received signal samples over the fading channel and after removing the CP can be expressed as:

$$y_n = h_\ell \circledast_N x_n + z_n, \quad 0 \leq n \leq N - 1, \quad (6)$$

where  $\{h_\ell\}_{\ell=0}^{L-1}$  is the  $L$ -tap channel impulse response,  $\circledast_N$  is the circular convolution operator with length  $N$ , and  $z_n$  is the time-domain additive white Gaussian noise (AWGN) represented in the expression PSD  $N_0/2$ . Hence, the received data at the  $k$ -th subcarrier is given as:

$$Y_k = H_k \cdot X_k + Z_k, \quad 0 \leq k \leq N - 1, \quad (7)$$

where  $Y_k$  and  $Z_k$  are the DFT of  $y_n$  and  $z_n$ , respectively, and  $H_k = \sum_{\ell=0}^{L-1} h_\ell W_N^{\ell k}$ ,  $0 \leq k \leq N - 1$  is the channel frequency response. By discarding the non-user data in  $Y_k$ . and applying  $M$ -point IDFT for the remaining components, the received symbols  $\{\hat{v}_m\}_{m=0}^{M-1}$  are obtained as:

$$\hat{v}_m = \sum_{k=0}^{M-1} Y_k W_M^{-km}, \quad 0 \leq m \leq M - 1. \quad (8)$$

Finally, the output PSK/QAM symbols by PCC-demapping are given as:

$$\hat{s}_r = \sum_{u=0}^{2^d-1} \hat{v}_{2^d r + u} \cdot (-1)^u, \quad 0 \leq r \leq P - 1. \quad (9)$$

Here, the value of  $d$  controls the growth of the symbol number in multiples of  $2^d$ , which is positively related to the ability of PAPR reduction. Therefore, the proposed PCC-DFT-s-OFDM provides the

flexibility of a trade-off between spectral efficiency and energy efficiency by adjusting the value of  $d$ , making the system more adaptive to the requirements of different communication scenarios.

### 3. Analysis of PCC-DFT-s-OFDM

#### 3.1. Time-Domain Aspect

Applying the moving average to the output of OFDM at transmitters is a simple and effective method for reducing the envelope fluctuation of OFDM signals (e.g., [27]). However, similar to other time-domain-oriented schemes, this causes severe inter-carrier-interference (ICI) and out-of-band radiation that degrades the performance of the BER and causes an adjacent channel leakage ratio because of the loss of orthogonality. In other words, a typical moving average is an exceptionally good smoothing filter, but an exceptionally poor low-pass filter. Despite this, PCC-DFT-s-OFDM can be introduced as a moving average-like technique while maintaining well frequency localization owing to its differential property [23]. To demonstrate this innovation in the time domain, we substituted (1) into (3) and obtained the following equation:

$$\begin{aligned}
 x_n &= \frac{1}{\sqrt{M}} \sum_{m=0}^{M-1} \left( s_m / 2^d \cdot (-1)^{m \bmod 2^d} \right) g \left[ n - \frac{N}{M} m \right] \\
 &= \frac{1}{\sqrt{M}} \sum_{r=0}^{P-1} s_r \cdot \sum_{u=0}^{2^d-1} (-1)^u g \left[ n - \frac{N}{M} (2^d r + u) \right] \\
 &= \frac{1}{\sqrt{M}} \sum_{r=0}^{P-1} s_r \cdot g_{n,r}^d, \quad 0 \leq n \leq N-1, \quad 0 \leq r \leq P-1,
 \end{aligned}
 \tag{10}$$

where  $g_{n,r}^d \triangleq \sum_{u=0}^{2^d-1} (-1)^u g \left[ n - \frac{N}{M} (2^d r + u) \right]$  is the transform of the filter, and  $g[n]$  still follows (4). Thus, it is clear that PCC-DFT-s-OFDM is a symbol set filtered by a  $2^d$ -tap smoothing filter.

Typical moving average filters are optimized to reduce random noise while retaining the sharpness of a step response. Hence, applying moving average filters to the PSK symbols would reduce PAPR more effectively when compared with using QAM symbols because of their constant envelope. The longer filter length and more rapid spatial roll-off of the former would result in a smoother (i.e., lower-PAPR) output signal.

Figure 2 plots the example transforms of  $g_{n,r}^d$  with  $N = 512$ ,  $M = 48$ , and  $d = 0, 1, 2, 3$ . As seen in Figure 2a,b, the transform of the conventional DFT-s-OFDM ( $g_{n,r}^0$ ) is a sinc-like function with a narrow main lobe and small roll-off. Figure 2c–h illustrate the transform of PCC-DFT-s-OFDM with different values of  $d$ . It can be seen that an increasing  $d$  widens the main lobe and concurrently suppresses the side lobe, exhibiting a desirable moving average filter.

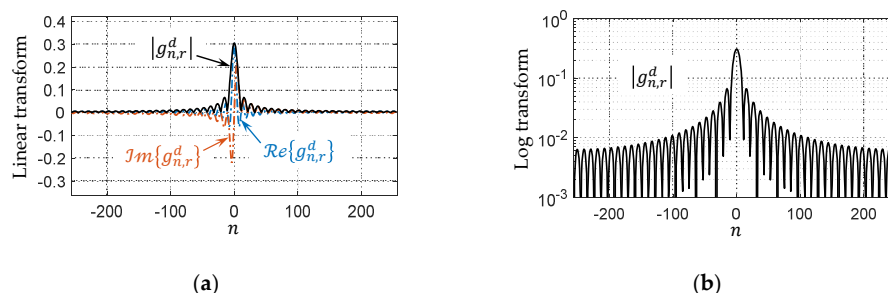
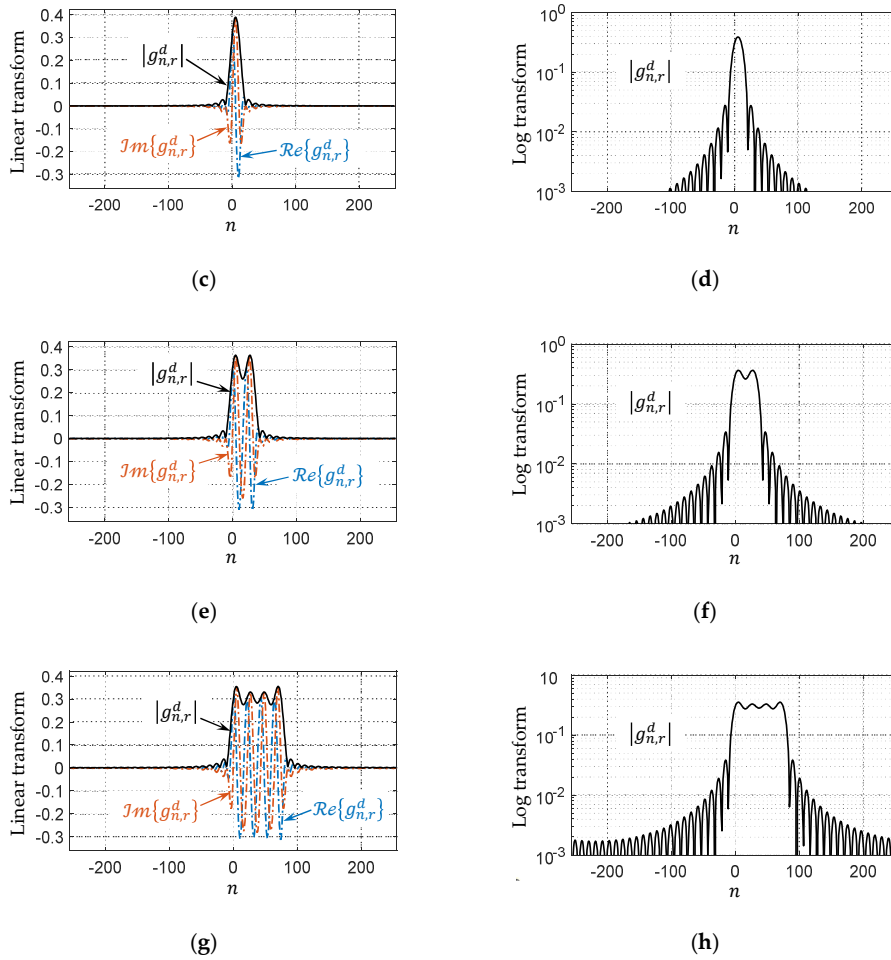


Figure 2. Cont.



**Figure 2.** Example transforms  $g_{n,r}^d$  with  $N = 512$  and  $M = 48$  for (a,b)  $d = 0$  (c,d)  $d = 1$  (e,f)  $d = 2$ , and (g,h)  $d = 3$ . Since  $g_{n,r}^d$  is complex-valued, its real/imaginary parts and amplitude (in linear/log scale) are shown separately.

### 3.2. Frequency-Domain Aspect

On the other hand, PCC-DFT-s-ODFM can be also regarded as a novel SS scheme for single-carrier waveform to reduce PAPR. Its shaping function can be derived by defining  $m = r + u$ ,  $0 \leq r \leq P - 1$ ,  $0 \leq u \leq 2^d - 1$  and substituting (1) into (2):

$$\begin{aligned}
 X_k &= \frac{1}{\sqrt{M}} \sum_{u=0}^{2^d-1} \sum_{r=0}^{P-1} (-1)^u s_r W_M^{k(r+u)} \\
 &= \sum_{u=0}^{2^d-1} (-W_M^k)^u \cdot \frac{1}{\sqrt{M}} \sum_{r=0}^{P-1} s_r W_P^{kr}, 0 \leq k \leq M - 1.
 \end{aligned}
 \tag{11}$$

Using (11), the PCC-based frequency-domain data vector can be expressed by multiplying the  $P$ -point DFT of  $\{s_r\}_{r=0}^{P-1}$  by a weighting sequence; that is, the PCC-based SS function. As  $d = 0$  (i.e.,  $P = M$ ) is an all-one sequence used to perform conventional DFT-s-OFDM, we consider  $d \in \{1, 2, \dots\}$  for the derived SS sequence  $G_k^d$  (the details are provided in Appendix A):

$$\begin{aligned}
 G_k^d &= \sum_{u=0}^{2^d-1} (-W_M^k)^u \\
 &= 2^d \sin\left(\frac{\pi k}{M}\right) \mathcal{G}[k] \cdot e^{j\frac{\pi}{2}} \prod_{p=1}^d W_M^{2^{d-p-1}k}, 0 \leq k \leq M - 1,
 \end{aligned}
 \tag{12}$$

where

$$\mathcal{G}[k] = \begin{cases} 1, & d = 1 \\ \prod_{p=1}^{d-1} \cos\left(\frac{2^{d-p}\pi k}{M}\right), & d > 1 \end{cases} \quad (13)$$

Equations (12) and (13) show how PCC-DFT-s-OFDM can be regarded as a novel complex-valued SS scheme instead of a real-value filter for DFT-s-OFDM. The PCC-based and spectral-shaped frequency components  $X_k^{PCC}$  can be obtained as a substitute for  $X_k$  as follows:

$$X_k^{PCC} = X_{k \bmod P}^P \cdot G_k^d, \quad 0 \leq k \leq M - 1, \quad (14)$$

where  $X_{k \bmod P}^P$  are the periodically extended coefficients of  $P$ -point DFT of  $\{v_r\}_{r=0}^{P-1}$ . Since (14) is basically an SS process, the frequency-domain data received after inverse-shaping  $Y_r^P$  at the receiver can be obtained using the equation [21]:

$$Y_r^P = \sum_{u=0}^{2^d-1} Y_{2^d r+u}^{PCC} \cdot G_{2^d r+u}^d, \quad 0 \leq r \leq P - 1, \quad (15)$$

where  $Y_{2^d r+u}^{PCC}$  is the received user data at the  $(2^d r + u)$ -th subcarrier. Although the number of transmitted symbols decreases from  $M$  to  $P$ , which shrinks spectral efficiency, the computational complexity of DFT is also decreased if we implement PCC-DFT-s-OFDM as an SS technique.

The example impulse responses of  $G_k^d$  with  $N = 512$ ,  $M = 48$ , and  $d = 1, 2, 3$  are depicted in Figure 3. As seen in Figure 3a,b,  $|G_k^1|$  is equivalent to the raised cosine (RC) spectrum-shaping vector [28] if  $d = 1$  is used for the proposed method and the roll-off factor is  $\beta = 1$  ( $\beta = 0-1$ ). This is because the half-sine curve in (12) is exactly consistent with the absolute value of the RC curve. For a higher-order SS, as shown in Figure 3c-f, shorter-period cosine curves described in (13) would be multiplied by the half-sine curve, making the signal spectrum more band-limited.

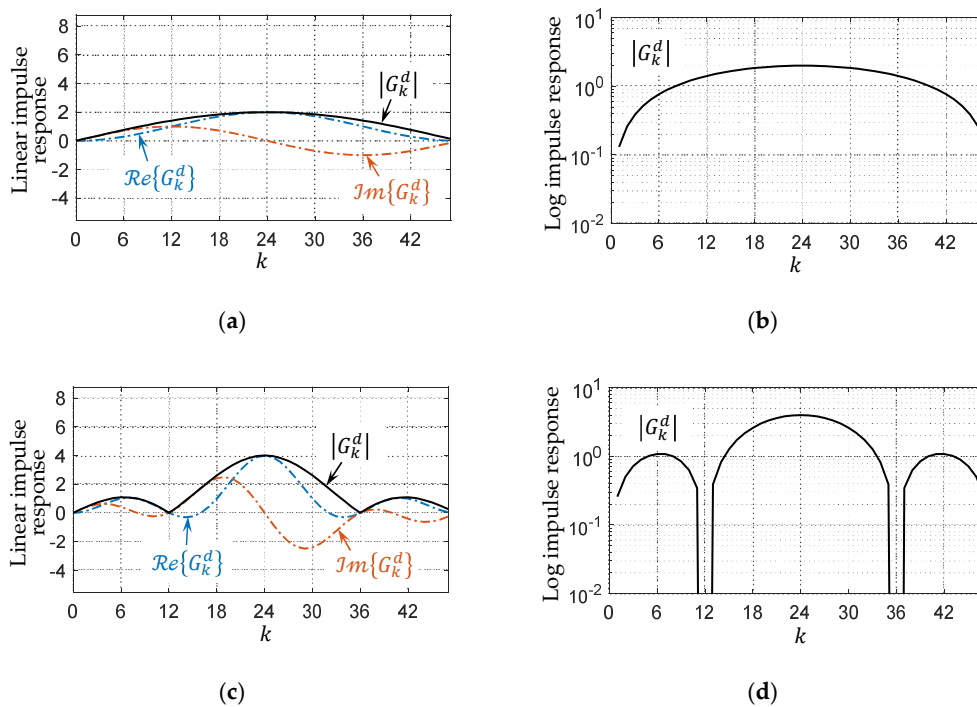
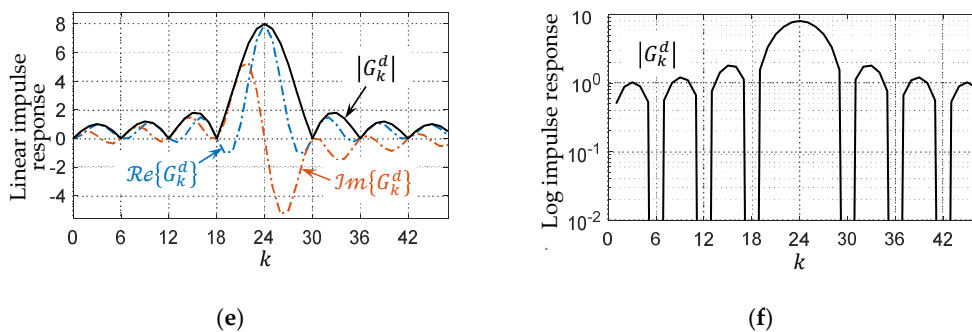


Figure 3. Cont.



**Figure 3.** Example impulse responses  $G_k^d$  with  $N = 512$  and  $M = 48$  for (a,b)  $d = 1$  (c,d)  $d = 2$ , and (e,f)  $d = 3$ . Since  $G_k^d$  is complex-valued, its real/imaginary parts and amplitude (in linear/log scale) are shown separately.

### 3.3. Computational Complexity

In this subsection, we analyze the computational complexity increase of PCC-based DFT precoding compared with conventional DFT precoding. According to (1) and (2), the PCC-based DFT precoded data vector  $\mathbf{X} = [X_0, \dots, X_{M-1}]^T$  can be rewritten as:

$$\mathbf{X} = \mathcal{F}_M \mathcal{P} \mathbf{s}, \tag{16}$$

where  $\mathcal{F}_M$  is the  $M$ -by- $M$  DFT matrix,  $\mathbf{s} = [s_0, \dots, s_{M-1}]^T$  is the input PSK/QAM symbol vector, and  $\mathcal{P}$  is an  $M$ -by- $P$  PCC mapping matrix whose entries are zeros except  $\mathcal{P}(2^d m, m) = (-1)^u, \dots, \mathcal{P}(2^d m + u, m) = (-1)^u$  for  $0 \leq m \leq M - 1$  and  $0 \leq u \leq 2^d - 1$ . The PCC demapping matrix is given by  $\mathcal{P}^\dagger$ , where  $[\cdot]^\dagger$  is the Moore-Penrose inverse. By mathematically evaluating the matrices  $\mathcal{P}$  and  $\mathcal{P}^\dagger$ , the PCC mapping and demapping increase  $M$  complex multiplications for the transmitter and  $P(2^d - 1) = M(1 - 2^{-d})$  complex additions for the receiver. However, since each PSK/QAM symbol only needs one complex multiplication to generate the results of  $d$ -order PCC-mapped symbols, the increased number of complex multiplications for the transmitter can be further reduced to  $P = M/2^d$ . Therefore, the comparison of computational complexity between conventional DFT precoder/deprefixer and PCC-based one can be summarized as Table 1. As seen, PCC-based DFT precoding requires  $\mathcal{O}(M^2)$  operations whose complexity is consistent with conventional DFT precoding, where  $\mathcal{O}(\cdot)$  is the Big-O notation. That is, the computational complexity increase of DFT precoding is almost negligible when PCC is applied. This makes PCC-DFT-s-OFDM more compatible with existing LTE/NR systems.

**Table 1.** Comparison of computational complexity between the conventional discrete Fourier transform (DFT) precoding and polynomial cancellation coding (PCC)-based DFT precoding.

Computational Complexity	Conventional DFT Precoding ( $d=0$ )		PCC-Based DFT Precoding ( $d>0$ )	
	Function	Big-O <sup>1</sup>	Function	Big-O <sup>1</sup>
Number of complex multiplications	Tx	$M^2$	$M2^{-d} + M^2$	$\mathcal{O}(M^2)$
	Rx	$M^2$	$M^2$	$\mathcal{O}(M^2)$
Number of complex additions	Tx	$M(M - 1)$	$M(M - 1)$	$\mathcal{O}(M^2)$
	Rx	$M(M - 1)$	$M(1 - 2^{-d}) + M(M - 1)$	$\mathcal{O}(M^2)$

<sup>1</sup> Both operations can be reduced to  $\mathcal{O}(M \log_2 M)$  if split-radix fast Fourier transform (FFT) is applied.

### 4. Simulation and Discussion

In this section, the performance of PCC-DFT-s-OFDM discrete baseband signals is evaluated in terms of PAPR, BER, and PSD, where the latter two also consider the scenarios of a single user (medium bandwidth only) and two users (medium bandwidth and narrow bandwidth). The system parameterization conforming to the 3GPP baseband standards [2,3] are listed in Table 2. In the simulations, the Rapp model for a solid state PA (SSPA) [29] with smoothness factor  $p = 2$  and 3 dB IBO are considered at the transmitter and perfect synchronization and channel estimation are assumed at the receiver. Furthermore, when  $d = 0$  in the proposed method, conventional DFT-s-OFDM is carried out.

Table 2. System parameterization.

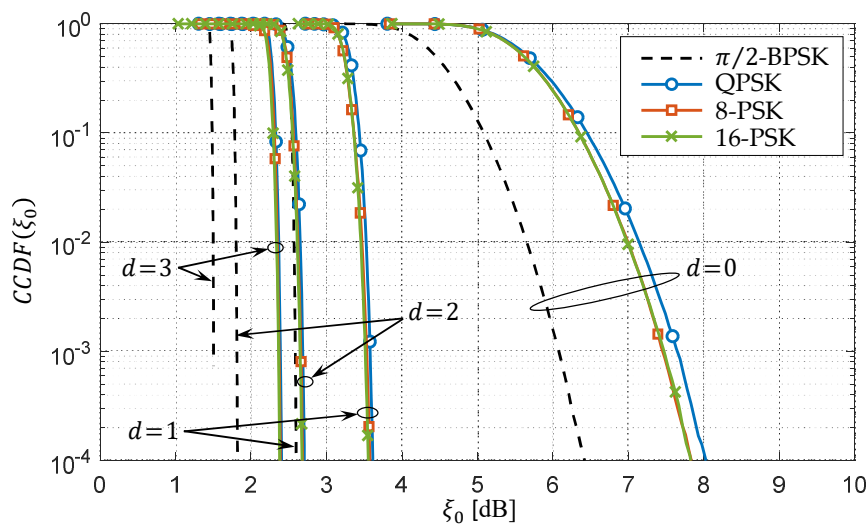
Parameter	Value
Carrier Bandwidth	10 MHz
Subcarrier Spacing	15 kHz
Fast Fourier Transform (FFT) Size ( $N$ )	1024
Number of allocated subcarriers for User 1 (medium bandwidth)	144 (12 PRBs)
Number of allocated subcarriers for User 2 (narrow bandwidth)	48 (4 PRBs)
Cyclic prefix (CP) length <sup>1</sup>	72
Modulation	$\pi/2$ -BPSK, QPSK, 16-QAM

<sup>1</sup> Length of channel impulse response ( $L$ ) is assumed to equal the CP length in the simulation.

#### 4.1. Peak-to-Average Power Ratio

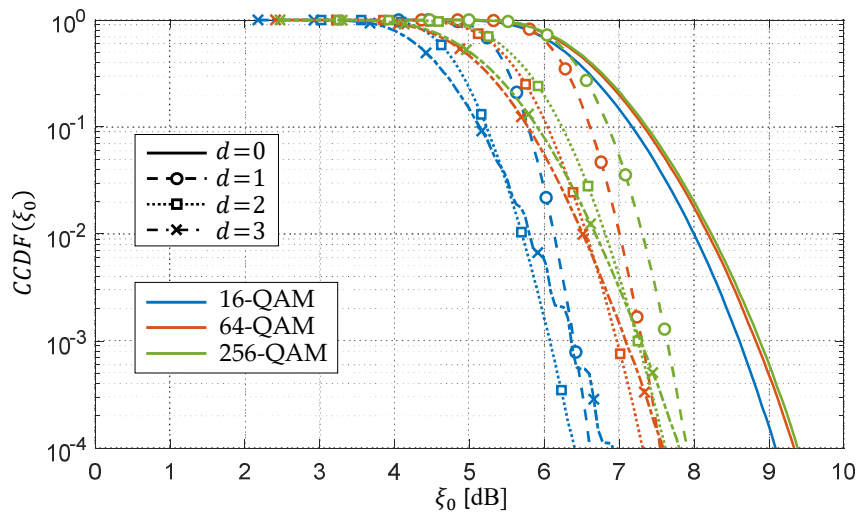
Figure 4 shows the PAPR CCDFs of PCC-DFT-s-OFDM at  $d = 0, 1, 2, 3$  for PSK and QAM signals. The PAPR performance of both signals improves significantly by changing  $d = 0$  to  $d = 1$ . In Figure 4a, the PAPR performances of all regular PSK signals appear similar for each given  $d$  and can be improved further as  $d$  increases. The PAPR performance curve of  $\pi/2$ -BPSK at  $d = 1$  almost overlaps that of the regular PSKs at  $d = 2$ . This indicates that the PAPR performance for  $\pi/2$ -BPSK is greatly superior to that of regular PSK.

However, Figure 4b shows that the improvements in the PAPR of QAM signals when  $d = 3$  are lower than when  $d = 2$ . This indicates that the PAPR performance is not always improved as  $d$  increases. This result supports the inferences made in Section 3.1 that PCC-DFT-s-OFDM filters provide a minor reduction in PAPR performance for dynamic-envelope symbols because they are moving average-like.



(a)

Figure 4. Cont.

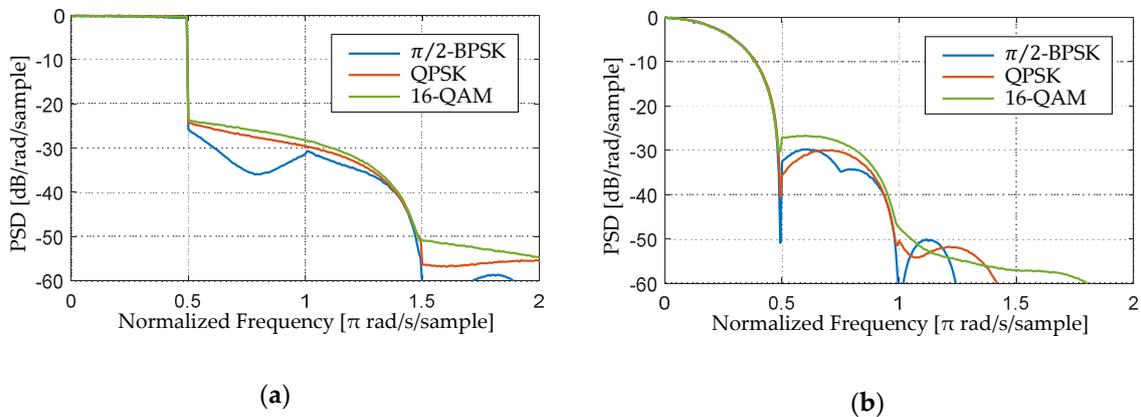


(b)

**Figure 4.** Complementary cumulative density function (CCDF) comparison of the peak-to-average power ratio (PAPR) at  $d = 0, 1, 2, 3$  for (a) phase shift keying (PSK) and (b) quadrature amplitude modulations (QAMs).

4.2. Power Spectral Density

Figure 5 shows the sub-band PSD performances of the PCC-DFT-s-OFDM at  $d = 0, 1, 2, 3$  for the  $\pi/2$ -BPSK, QPSK, and 16-QAM signals. The maximum power for each simulation was normalized to 0 dB to ensure a fair comparison. As  $d$  increased, the proposed method concentrated the in-band spectrum and diminished the out-of-band energy. Furthermore, the latter effect would be obvious if PA was considered. Although the PAPR performances of these three kinds of modulations were quite different, their extent of spectrum spreading due to nonlinear distortion was similar. This means that even for low-order/PAPR modulations in DFT-s-OFDM (i.e.,  $\pi/2$ -BPSK and QPSK), there is still only limited improvement for PSD when PA nonlinearity is concerned. The advantage of lessening the out-of-band radiation can be underlined from the inter-user interference perspective. As seen in Figure 6a, the side-lobes of two spectrum-adjacent users severely influence the main-lobe of each other when  $d = 0$ . Figure 6b–d displays the mitigation of ICI for  $d = 1, 2, 3$ ; as  $d$  increases, the main-beams of the two users increasingly separate and their PSDs overlap less; that is, lower interference plus noise ratio (SINR) is achieved. Such SINR improvement is especially significant when more users are considered.



(a)

(b)

**Figure 5.** Cont.

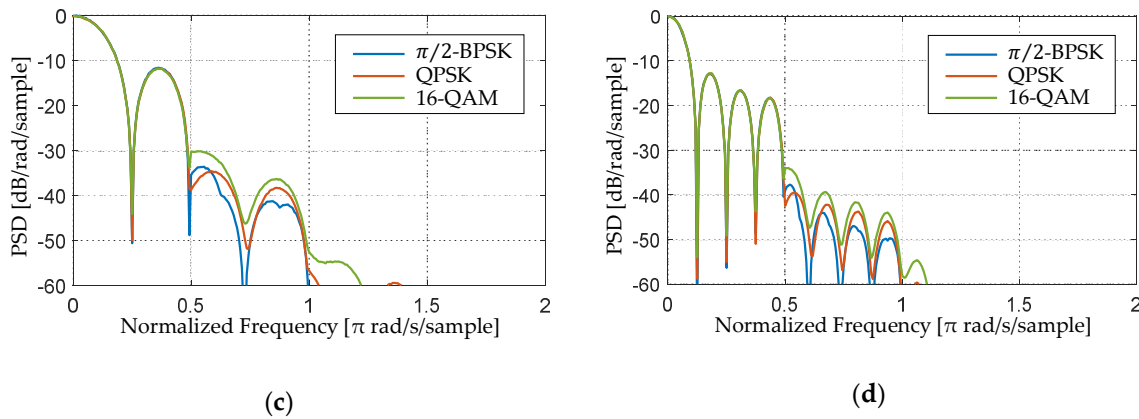


**Figure 5.** Single-user power spectral density (PSD) performances of polynomial cancellation coded (PCC) discrete Fourier transform-spread orthogonal frequency division multiplexing (DFT-s-OFDM) for different modulations at (a)  $d = 0$ , (b)  $d = 1$ , (c)  $d = 2$ , and (d)  $d = 3$ .

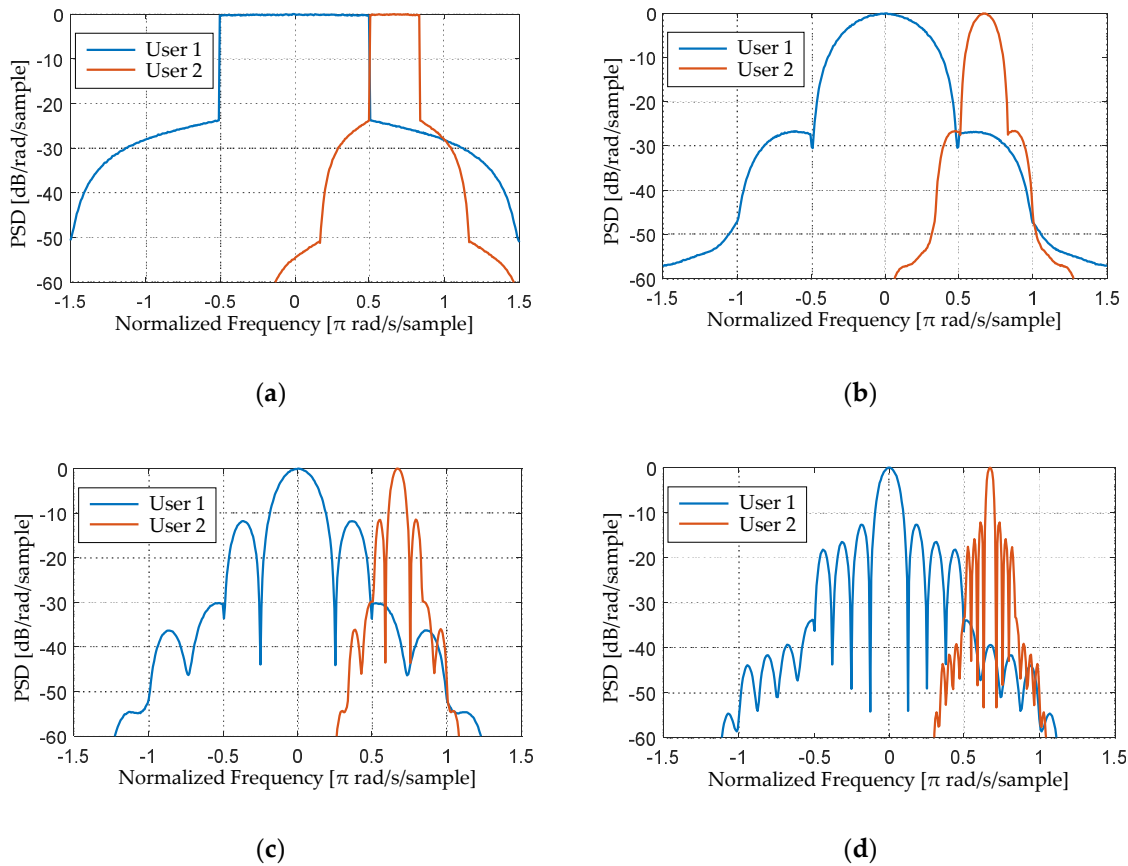


**Figure 6.** Two-user power spectral density (PSD) performances of polynomial cancellation coded (PCC) discrete Fourier transform-spread orthogonal frequency division multiplexing (DFT-s-OFDM) for 16-quadrature amplitude modulation (16-QAM) signals at (a)  $d = 0$ , (b)  $d = 1$ , (c)  $d = 2$ , and (d)  $d = 3$ . The frequency is normalized to User 1’s bandwidth.

### 4.3. Bit Error Rate

Figure 7 shows uncoded BER performance comparisons of PCC-DFT-s-OFDM over the AWGN channel at  $d = 0, 1, 2, 3$  for single-user  $\pi/2$ -BPSK, QPSK, and 16-QAM signals. When  $\pi/2$ -BPSK at  $d = 0$ , the BER curve is almost identical to the lower bound, implying that  $\pi/2$ -BPSK has a high tolerance for PA nonlinearity. For QPSK, there is a slight degradation in BER at  $d = 0$ . However, its performance

can be improved to match the lower bound at  $d = 1$ . For 16-QAM, the BER improvement is remarkable at  $d = 1, 2$  but moderate at  $d = 3$  owing to the inferior PAPR performance.

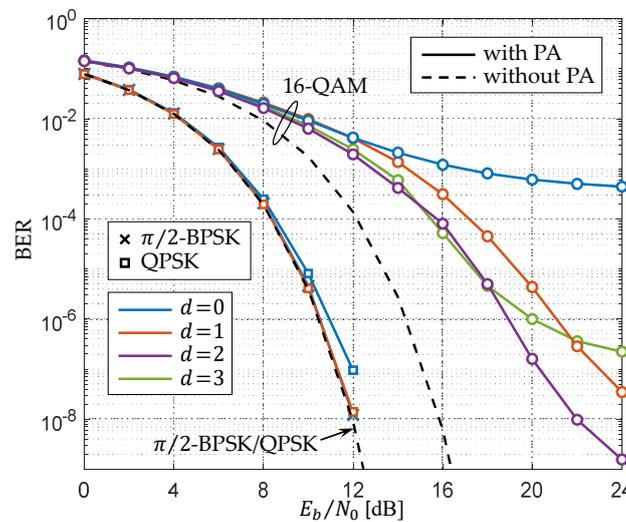


**Figure 7.** Single-user bit error rate (BER) performances of polynomial cancellation coded (PCC) discrete Fourier transform-spread orthogonal frequency division multiplexing (DFT-s-OFDM) over the additive white Gaussian noise (AWGN) channel for different values of  $d$ .

Figure 8, Tables 3 and 4 show the BER results over AWGN and Rayleigh fading channel. The performance of 16-QAM signals improves significantly at  $d = 1$  while appearing close to the undistorted signals at  $d = 2, 3$ . The results for  $\pi/2$ -BPSK and QPSK are almost the same as those for the undistorted signals at each value of  $d$ . Despite this, it is interesting that the proposed method essentially enhances the immunity of DFT-s-OFDM to frequency-selective fading thanks to a property akin to the SS technique. As shown in Figure 3, the band of the PCC-DFT-s-OFDM signals becomes narrower through the higher order of PCC symbols, mitigating the interference from the frequency-selective fading channel.

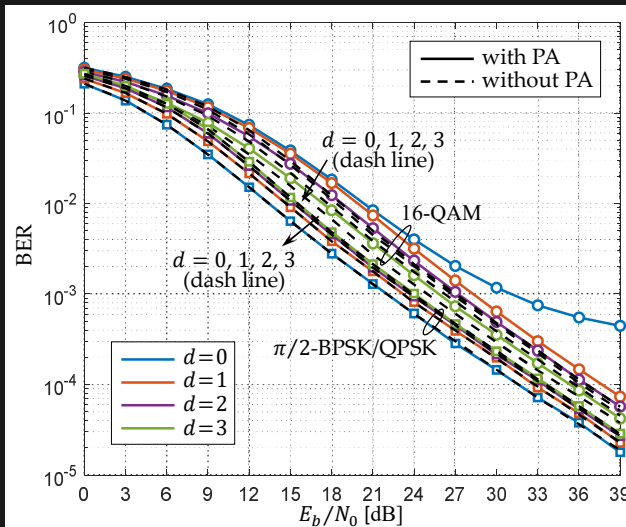


**Figure 8.** Single-user bit error rate (BER) performances of polynomial cancellation coded (PCC) discrete Fourier transform-spread orthogonal frequency division multiplexing (DFT-s-OFDM) over additive white Gaussian noise (AWGN) and Rayleigh fading channel for different values of  $d$ .

**Table 3.** Single-user bit error rate (BER) performances of the proposed method for the quadrature phase shift keying (QPSK) signal over additive white Gaussian noise (AWGN) and Rayleigh fading channel for different values of  $d$ .

$E_b/N_0$ (dB)	Without PA Nonlinearity				With PA Nonlinearity			
	$d=0$	$d=1$	$d=2$	$d=3$	$d=0$	$d=1$	$d=2$	$d=3$
12	$2.896 \times 10^{-2}$	$2.599 \times 10^{-2}$	$2.156 \times 10^{-2}$	$1.516 \times 10^{-2}$	$2.965 \times 10^{-2}$	$2.614 \times 10^{-2}$	$2.162 \times 10^{-2}$	$1.523 \times 10^{-2}$
21	$2.143 \times 10^{-3}$	$1.958 \times 10^{-3}$	$1.782 \times 10^{-3}$	$1.290 \times 10^{-3}$	$2.157 \times 10^{-3}$	$1.971 \times 10^{-3}$	$1.896 \times 10^{-3}$	$1.331 \times 10^{-3}$
30	$2.325 \times 10^{-4}$	$2.145 \times 10^{-4}$	$1.938 \times 10^{-4}$	$1.450 \times 10^{-4}$	$2.354 \times 10^{-4}$	$2.206 \times 10^{-4}$	$2.972 \times 10^{-4}$	$1.461 \times 10^{-4}$
39	$2.841 \times 10^{-5}$	$2.681 \times 10^{-5}$	$2.268 \times 10^{-5}$	$1.785 \times 10^{-5}$	$2.867 \times 10^{-5}$	$2.715 \times 10^{-5}$	$2.289 \times 10^{-5}$	$1.886 \times 10^{-5}$

**Table 4.** Single-user bit error rate (BER) performances of the proposed method for the 16-quadrature amplitude modulation (16-QAM) signal over additive white Gaussian noise (AWGN) and Rayleigh fading channel for different values of  $d$ .

$E_b/N_0$ (dB)	Without PA Nonlinearity				With PA Nonlinearity			
	$d=0$	$d=1$	$d=2$	$d=3$	$d=0$	$d=1$	$d=2$	$d=3$
12	$6.483 \times 10^{-2}$	$5.822 \times 10^{-2}$	$4.841 \times 10^{-2}$	$3.492 \times 10^{-2}$	$7.388 \times 10^{-2}$	$6.854 \times 10^{-2}$	$5.537 \times 10^{-2}$	$4.069 \times 10^{-2}$
21	$5.007 \times 10^{-3}$	$4.488 \times 10^{-3}$	$3.859 \times 10^{-3}$	$2.712 \times 10^{-3}$	$8.412 \times 10^{-3}$	$7.393 \times 10^{-3}$	$5.330 \times 10^{-3}$	$3.629 \times 10^{-3}$
30	$4.802 \times 10^{-4}$	$4.593 \times 10^{-4}$	$3.865 \times 10^{-4}$	$2.930 \times 10^{-4}$	$1.175 \times 10^{-3}$	$6.408 \times 10^{-4}$	$4.925 \times 10^{-4}$	$3.543 \times 10^{-4}$
39	$5.693 \times 10^{-5}$	$5.147 \times 10^{-5}$	$4.537 \times 10^{-5}$	$3.781 \times 10^{-5}$	$4.64 \times 10^{-4}$	$7.340 \times 10^{-5}$	$5.706 \times 10^{-5}$	$4.217 \times 10^{-5}$

Figure 9 presents the BER performances of two spectrum-adjacent users whose PSD refer to Figure 6. Clearly, serious BER degradation was found when inter-user interference is further considered. By applying PCC to DFT-s-OFDM, the BER of both users is greatly improved because their side-lobes have been suppressed to avoid interfering with the main-beam of each other. However, since more allocated bandwidth causes a greater side-lobe component than that of other users, the BER of User 1 mainly improves at  $d = 1$  (see Figure 9a,c) while that of User 2 mainly improves at  $d = 2$  (see Figure 9b,d).

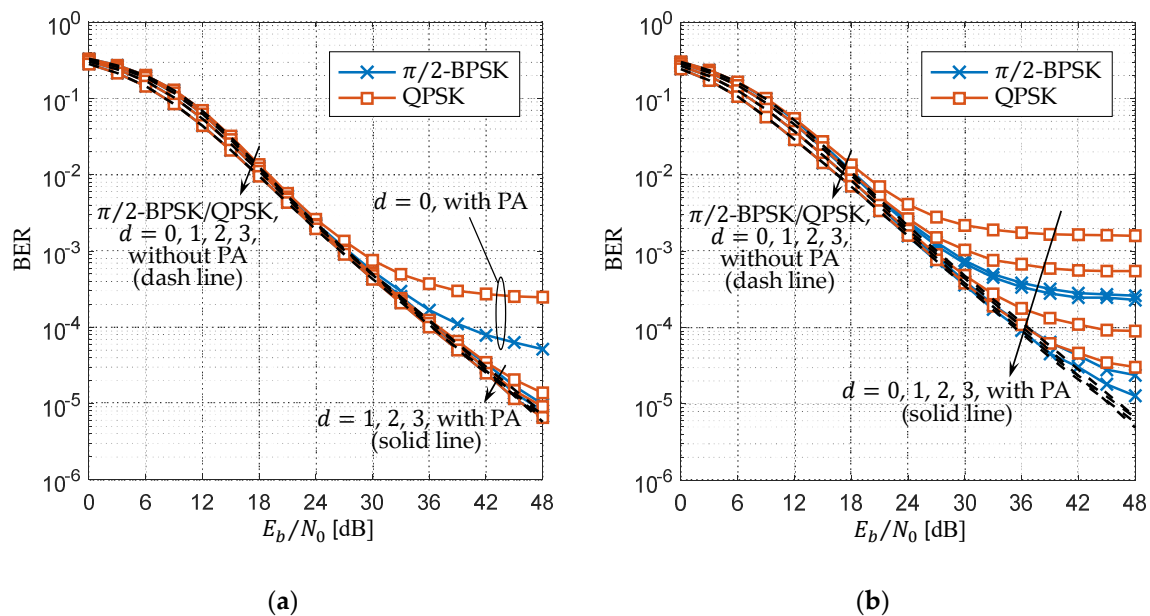
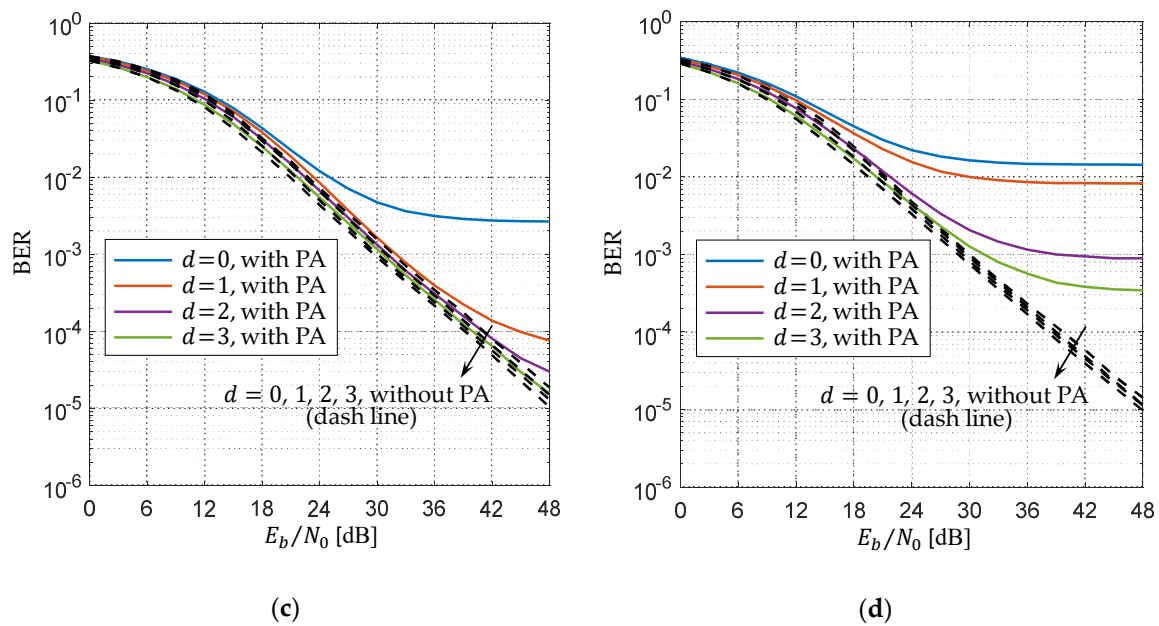


Figure 9. Cont.



**Figure 9.** Two-user bit error rate (BER) performances of polynomial cancellation coded (PCC) discrete Fourier transform-spread orthogonal frequency division multiplexing (DFT-s-OFDM) over the Rayleigh channel for different values of  $d$  for (a) User 1 (with medium bandwidth) for  $\pi/2$ -binary phase shift keying (BPSK) and quadrature PSK (QPSK), (b) User 2 (with narrow bandwidth) for  $\pi/2$ -BPSK and QPSK, (c) User 1 for 16-quadrature amplitude modulation (QAM), and (d) User 2 for 16-QAM.

#### 4.4. Discussion

The simulation results show that the BER enhancement is evident even for low-order modulations (i.e.,  $\pi/2$ -BPSK and QPSK) if both PA nonlinearity and inter-user interference are considered. Furthermore, the proposed method can effectively improve PSD performance and the immunity of the frequency-selective fading channel for all modulations in DFT-s-OFDM systems that benefit from the transformed-domain data localization of PCC symbols. The extent of the improvement for PAPR, PSD and BER performances depends on the value of  $d$ , which would decrease data rate  $2^d$  times. Indeed, this might be the main drawback of the proposed method. However, aiming to improve the flexibility on the trade-off between spectral efficiency and the other performances for DFT-s-OFDM, the proposed architecture creates the opportunity for further improvement in terms of PAPR, PSD and BER performances when the channel condition allows bandwidth-greedy transmission. Otherwise, one can reduce to the conventional DFT-s-OFDM for the transmission by using  $d = 0$ .

#### 5. Conclusions

As 5G services bring more diverse communication scenarios, low-PAPR LTE-legacy uplink signaling, DFT-s-OFDM, requires greater flexibility in its PAPR performance for adapting miscellaneous 5G devices. We have proposed a generalized PCC technique to solve the inflexibility of regulating the PAPR of DFT-s-OFDM uplink signals by reducing the PAPR in a controllable manner. By deriving the SS function for PCC-DFT-s-OFDM, we have proved that the proposed method can be considered as a novel SS technique for DFT-s-OFDM. Based on the cost of spectral efficiency, which might be a relatively tolerable requirement for URLLC, mMTC, and D2D ProSe in LTE/NR, the simulation results show that our PCC-DFT-s-OFDM outperforms the conventional DFT-s-OFDM in terms of PAPR, PSD, and BER, the last especially with the inter-user interference. Hence, our method is the most suitable to support the various D2D transmissions and URLLC/mMTC services.

Owing to the low complexity of PCC, future work could evaluate the combination of PCC and current uplink/downlink signaling options (i.e., DFT-s-OFDM/CP-OFDM) as potential waveform

candidates for 5G and beyond. Such combinations can include other advantages of PCC-OFDM, such as the reduction of ICI [30], enhancement for MIMO systems [31,32], and increasing the robustness of asynchronous communications [33,34], forming a highly flexible PCC-/DFT-s-/OFDM system against the complicated 5G environment.

**Author Contributions:** Conceptualization, L.C. and Y.-S.W.; Software and Validation, L.C. and Y.-M.K.; Formal Analysis, L.C.; Writing—Original Draft Preparation, Review and Editing, L.C. and C.-Y.H.; Supervision, C.-Y.H.

**Funding:** This work was supported in part by Industrial Technology Research Institute, Taiwan, under grant number V1-107001.

**Acknowledgments:** The authors would like to thank the Editor and the anonymous reviewers for their valuable comments and suggestions.

**Conflicts of Interest:** The authors declare no conflict of interest.

### Appendix A. Spectral Shaping Function of PCC-DFT-s-OFDM

For the  $d$ -order PCC-DFT-s-OFDM, its SS function,  $G_k^d = \sum_{u=0}^{2^d-1} (-W_M^k)^u$ ,  $0 \leq k \leq M-1$ , can be extracted by (11) and rewritten as follows:

$$\begin{aligned}
 G_k^d &= \sum_{u=0}^{2^d-1} (-W_M^k)^u = \frac{1 - (-W_M^k)^{2^d}}{1 + W_M^k} = \frac{1 - W_M^{2^d k}}{1 + W_M^k} \\
 &= \frac{(1 + W_M^{2^d-1 k})(1 + W_M^{2^d-2 k}) \dots (1 + W_M^{2^d-d k})(1 - W_M^{2^d-d k})}{1 + W_M^k} \\
 &= (1 - W_M^k) \prod_{p=1}^{d-1} (1 + W_M^{2^{d-p} k}) \\
 &= 2j \cdot W_M^{\frac{k}{2}} \left( \frac{W_M^{-\frac{k}{2}} - W_M^{\frac{k}{2}}}{2j} \right) \prod_{p=1}^{d-1} W_M^{2^{d-p-1} k} 2 \cos\left(\frac{W_M^{2^{d-p-1} k} + W_M^{2^{d-p-1} k}}{2}\right) \\
 &= 2j \cdot W_M^{\frac{k}{2}} \sin\left(\frac{2\pi}{M} \times \frac{k}{2}\right) \prod_{p=1}^{d-1} W_M^{2^{d-p-1} k} 2 \cos\left(\frac{2\pi}{M} \times 2^{d-p-1} k\right) \\
 &= 2^d \underbrace{\sin\left(\frac{\pi k}{M}\right) \prod_{p=1}^{d-1} \cos\left(\frac{2^{d-p} \pi k}{M}\right)}_{\text{Amplitude Response}} e^{j\frac{\pi}{2}} \underbrace{\prod_{p=1}^d W_M^{2^{d-p-1} k}}_{\text{Phase Response}}, 0 \leq k \leq M-1.
 \end{aligned} \tag{A1}$$

Since the term of  $\prod_{p=1}^{d-1} \cos\left(\frac{2^{d-p} \pi k}{M}\right)$  in the amplitude response is invalid if  $d = 1$ , we define a function  $\mathcal{G}[k]$  described in (13) for the validity. Consequently, (12) is derived.

### References

1. Hwang, T.; Yang, C.; Wu, G.; Li, S.; Li, G.Y. OFDM and Its Wireless Applications: A Survey. *IEEE Trans. Veh. Technol.* **2009**, *58*, 1673–1694. [CrossRef]
2. 3GPP. TS 36.211 V15.7.0. In *Technical Specification Group Radio Access Network; Physical Channels and Modulation (Release 15)*; 3rd Generation Partnership Project: Newport Beach, CA, USA, 2019.
3. 3GPP. TS 38.211 V15.7.0. In *Technical Specification Group Radio Access Network; Physical Channels and Modulation (Release 15)*; 3rd Generation Partnership Project: Newport Beach, CA, USA, 2019.
4. Wunder, G.; Fischer, R.F.H.; Boche, H.; Litsyn, S.; No, J.-S. The PAPR Problem in OFDM Transmission: New Directions for a Long-Lasting Problem. *IEEE Signal Process. Mag.* **2013**, *30*, 130–144. [CrossRef]
5. Han, S.H.; Lee, J.H. An overview of peak-to-average power ratio reduction techniques for multicarrier transmission. *IEEE Wirel. Commun.* **2005**, *12*, 56–65. [CrossRef]
6. Jiang, T.; Wu, Y. An Overview: Peak-to-Average Power Ratio Reduction Techniques for OFDM Signals. *IEEE Trans. Broadcast.* **2008**, *54*, 257–268. [CrossRef]

7. Rahmatallah, Y.; Mohan, S. Peak-To-Average Power Ratio Reduction in OFDM Systems: A Survey And Taxonomy. *IEEE Commun. Surv. Tutor.* **2013**, *15*, 1567–1592. [CrossRef]
8. Sandoval, F.; Poitau, G.; Gagnon, F. Hybrid Peak-to-Average Power Ratio Reduction Techniques: Review and Performance Comparison. *IEEE Access* **2017**, *5*, 27145–27161. [CrossRef]
9. Nokia, Alcatel-Lucent Shanghai Bell. Potential for System Level Gains with Low PAPR Waveforms, R1-167795. 2016. Available online: [https://www.3gpp.org/ftp/tsg\\_ran/WG1\\_RL1/TSGR1\\_86/Docs/R1-167795.zip](https://www.3gpp.org/ftp/tsg_ran/WG1_RL1/TSGR1_86/Docs/R1-167795.zip) (accessed on 31 October 2019).
10. Zaidi, A.A.; Baldemair, R.; Tullberg, H.; Bjorkegren, H.; Sundstrom, L.; Medbo, J.; Kilinc, C.; Da Silva, I. Waveform and Numerology to Support 5G Services and Requirements. *IEEE Commun. Mag.* **2016**, *54*, 90–98. [CrossRef]
11. Ankarali, Z.E.; Pekoz, B.; Arslan, H. Flexible Radio Access Beyond 5G: A Future Projection on Waveform, Numerology, and Frame Design Principles. *IEEE Access* **2017**, *5*, 18295–18309. [CrossRef]
12. Demir, A.F.; Elkourdi, M.; Ibrahim, M.; Arslan, H. Waveform Design for 5G and Beyond. In *5G Networks: Fundamental Requirements, Enabling Technologies, and Operations Management*; John Wiley & Sons, Inc.: Hoboken, NJ, USA, 2018; pp. 51–76.
13. Farhang-Boroujeny, B.; Moradi, H. OFDM Inspired Waveforms for 5G. *IEEE Commun. Surv. Tutor.* **2016**, *18*, 2474–2492. [CrossRef]
14. Myung, H.; Lim, J.; Goodman, D. Single carrier FDMA for uplink wireless transmission. *IEEE Veh. Technol. Mag.* **2006**, *1*, 30–38. [CrossRef]
15. 3GPP. TS 36.211 V13.3.0. In *Technical Specification Group Radio Access Network; Physical Channels and Modulation (Release 13)*; 3rd Generation Partnership Project: New Orleans, LA, USA, 2016.
16. Cho, L.; Liao, H.-C.; Hsu, C.-Y. Adjustable PAPR reduction for DFT-s-OFDM via improved general precoding scheme. *Electron. Lett.* **2018**, *54*, 903–905. [CrossRef]
17. International Telecommunication Union (ITU). *IMT Vision—Framework and Overall Objectives of the Future Development of IMT for 2020 and Beyond*; ITU-R: Geneva, Switzerland, 2015; p. 21.
18. 3GPP. TS 23.303 V15.1.0. In *Technical Specification Group Services and System Aspects; Technical Specification Group Services and System Aspects; Proximity-Based Services (ProSe); Stage 2 (Release 15)*; 3rd Generation Partnership Project: La Jolla, CA, USA, 2018.
19. Hori, Y.; Ochiai, H. A New Uplink Multiple Access Based on OFDM With Low PAPR, Low Latency, and High Reliability. *IEEE Trans. Commun.* **2018**, *66*, 1996–2008. [CrossRef]
20. Mauritz, O.; Popovic, B. Optimum Family of Spectrum-Shaping Functions for PAPR Reduction of DFT-Spread OFDM Signals. In *Proceedings of the IEEE Vehicular Technology Conference (VTC-Fall)*, Montreal, QC, Canada, 25–28 September 2006; pp. 1–5.
21. Hsu, C.-Y.; Liao, H.-C. Generalised precoding method for PAPR reduction with low complexity in OFDM systems. *IET Commun.* **2018**, *12*, 796–808. [CrossRef]
22. Armstrong, J.; Grant, P.M.; Povey, G. Polynomial cancellation coding of OFDM to reduce intercarrier interference due to Doppler spread. In *Proceedings of the IEEE Global Telecommun. Conf. (GLOBECOM)*, Sydney, Australia, 8–12 November 1998; pp. 2771–2776.
23. Kongara, G.; Yang, L.; He, C.; Armstrong, J. A Comparison of CP-OFDM, PCC-OFDM and UFMC for 5G Uplink Communications. *IEEE Access* **2019**, *7*, 157574–157594. [CrossRef]
24. Bäuml, R.W.; Fischer, R.F.H.; Huber, J.B. Reducing the peak-to-average power ratio of multicarrier modulation by selected mapping. *Electron. Lett.* **1996**, *32*, 2056–2057. [CrossRef]
25. Müller, S.H.; Huber, J.B. OFDM with reduced peak-to-average power ratio by optimum combination of partial transmit sequences. *Electron. Lett.* **1997**, *33*, 368–369. [CrossRef]
26. Ochiai, H. On Instantaneous Power Distributions of Single-Carrier FDMA Signals. *IEEE Wirel. Commun. Lett.* **2012**, *1*, 73–76. [CrossRef]
27. Ali, H.; Yaqub, R. A Low Complexity Linear Moving Average Filtering Technique for PAR Reduction in OFDM Systems. *Int. J. Commun. Netw. Syst. Sci.* **2018**, *11*, 199–215. [CrossRef]
28. Samsung. Frequency Domain Spectrum Shaping for DFT-s-OFDM, R1-1703016. 2017. Available online: [https://www.3gpp.org/ftp/tsg\\_ran/WG1\\_RL1/TSGR1\\_88/Docs/R1-1703016.zip](https://www.3gpp.org/ftp/tsg_ran/WG1_RL1/TSGR1_88/Docs/R1-1703016.zip) (accessed on 31 October 2019).
29. Rapp, C. Effect of HPA-nonlinearity on 4-DPSK/OFDM-signal for a digital sound broadcasting system. In *Proceedings of the 2nd European Conf. Satellite Commun. (ECSC)*, Liege, Belgium, 22–24 October 1991; pp. 179–184.

30. Ryu, H.-G.; Li, Y.; Park, J.-S. An Improved ICI Reduction Method in OFDM Communication System. *IEEE Trans. Broadcast.* **2005**, *51*, 395–400. [[CrossRef](#)]
31. Tang, T.; Zhang, Y.; Jiang, J.; Zhang, P. A MIMO-PCC-OFDM System for Multipath Fading Channels with Carrier Frequency Offset. In Proceedings of the Int. Symp. Commun. and Inform. Technol. (ISCIT), Bangkok, Thailand, 18–20 October 2006; pp. 511–515.
32. Li, X.; Armstrong, J. An Improved MIMO PCC OFDM System with Reduced Sensitivity to Imperfect CSI. In Proceedings of the IEEE Wirel. Commun. and Netw. Conf. (WCNC), Sydney, Australia, 18–21 April 2010; pp. 1–6.
33. Wang, S.; Armstrong, J.; Thompson, J.S. Waveform performance for asynchronous wireless 5G uplink communications. In Proceedings of the IEEE 27th Annu. Int. Symp. Personal, Indoor, and Mobile Radio Commun. (PIMRC), Valencia, Spain, 4–8 September 2016; pp. 1–6.
34. Wang, S.; Thompson, J.S.; Grant, P.M. Closed-Form Expressions for ICI/ISI in Filtered OFDM Systems for Asynchronous 5G Uplink. *IEEE Trans. Commun.* **2017**, *65*, 4886–4898. [[CrossRef](#)]



© 2019 by the authors. Licensee MDPI, Basel, Switzerland. This article is an open access article distributed under the terms and conditions of the Creative Commons Attribution (CC BY) license (<http://creativecommons.org/licenses/by/4.0/>).